



**HAL**  
open science

## Temporal focusing with spatially modulated excitation

Eirini Papagiakoumou, Vincent de Sars, Valentina Emiliani, Dan Oron

► **To cite this version:**

Eirini Papagiakoumou, Vincent de Sars, Valentina Emiliani, Dan Oron. Temporal focusing with spatially modulated excitation. *Optics Express*, 2009, 17 (7), pp.5391-5401. 10.1364/OE.17.005391 . hal-01963255

**HAL Id: hal-01963255**

**<https://hal.science/hal-01963255>**

Submitted on 21 Dec 2018

**HAL** is a multi-disciplinary open access archive for the deposit and dissemination of scientific research documents, whether they are published or not. The documents may come from teaching and research institutions in France or abroad, or from public or private research centers.

L'archive ouverte pluridisciplinaire **HAL**, est destinée au dépôt et à la diffusion de documents scientifiques de niveau recherche, publiés ou non, émanant des établissements d'enseignement et de recherche français ou étrangers, des laboratoires publics ou privés.

# Temporal focusing with spatially modulated excitation

Eirini Papagiakoumou<sup>a</sup>, Vincent de Sars<sup>a</sup>, Valentina Emiliani<sup>a</sup>, and Dan Oron<sup>b</sup>

<sup>a</sup> *Neurophysiology and New Microscopies Laboratory: Wavefront engineering microscopy group, CNRS UMR8154, INSERM S603, Paris Descartes University, 45 rue des Saints Peres, 75270 Paris Cedex 06, France*

<sup>b</sup> *Department of Physics of Complex Systems, Weizmann Institute of Science, Rehovot, Israel*  
[dan.aron@weizmann.ac.il](mailto:dan.aron@weizmann.ac.il)

**Abstract:** Temporal focusing of ultrashort pulses has been shown to enable wide-field depth-resolved two-photon fluorescence microscopy. In this process, an entire plane in the sample is selectively excited by introduction of geometrical dispersion to an ultrashort pulse. Many applications, such as multiphoton lithography, uncaging or region-of-interest imaging, require, however, illumination patterns which significantly differ from homogeneous excitation of an entire plane in the sample. Here we consider the effects of such spatial modulation of a temporally focused excitation pattern on both the generated excitation pattern and on its axial confinement. The transition in the axial response between line illumination and wide-field illumination is characterized both theoretically and experimentally. For 2D patterning, we show that in the case of amplitude-only modulation the axial response is generally similar to that of wide-field illumination, while for phase-and-amplitude modulation the axial response slightly deteriorates when the phase variation is rapid, a regime which is shown to be relevant to excitation by beams shaped using spatial light modulators. Finally, general guidelines for the use of spatially modulated temporally focused excitation are presented.

© 2009 Optical Society of America

**OCIS codes:** (090.1995) Digital holography; (180.4315) Non-linear microscopy

---

## References and links

1. W. Denk, J. H. Strickler, and W. W. Webb, "Two-photon laser scanning fluorescence microscopy," *Science* **248**, 73-76 (1990).
2. R. R. Gattass and E. Mazur, "Femtosecond laser micromachining in transparent materials," *Nature Photonics* **2**, 219-225 (2008).
3. X. Lv, C. Zhan, S. Zeng, W. R. Chen, and Q. Luo, "Construction of multiphoton laser scanning microscope based on dual-axis acousto-optic deflector," *Rev. Sci. Instr.* **77**, 046101 (2006) and references therein.
4. G. D. Reddy, K. Kelleher, R. Fink, and P. Saggau, "Three-dimensional random access multiphoton microscopy for functional imaging of neuronal activity," *Nature Neuroscience* **11**, 713-720 (2008).
5. B. Judkewitz, A. Roth, and M. Hausser, "Dendritic enlightenment: using patterned two-photon uncaging to reveal the secrets of the brain's smallest dendrites," *Neuron* **50**, 180-183 (2006)
6. A. H. Buist, M. Muller, J. Squier, and G. J. Brakenhoff, "Real-time two-photon absorption microscopy using multipoint excitation," *J. Microsc.* **192**, 217-226 (1998).
7. J. Bewersdorf, R. Pick, and S. W. Hell, "Multifocal multiphoton microscopy," *Opt. Lett.* **23**, 655-657 (1998)
8. D. N. Fittinghoff, P. W. Wiseman, and J. A. Squier, "Widefield multiphoton and temporally decorrelated multifocal multiphoton microscopy," *Opt. Express* **7**, 273-279 (2000).

9. T. Nielsen, M. Fricke, D. Hellweg, and P. Andresen, "High efficiency beam splitter for multifocal multiphoton microscopy," *J. Microsc.* **201**, 368-376 (2001).
10. V. Nikolenko, K. E. Poskanzer, and R. Yuste, "Two-photon photostimulation and imaging of neural circuits," *Nat. Methods* **4**, 943-950 (2007).
11. C. Lutz, T. S. Otis, V. de Sars, S. Charpak, D. A. DiGregorio, and V. Emiliani, "Holographic photolysis of caged neurotransmitters," *Nat. Methods* **5**, 821-827 (2008).
12. D. Oron, E. Tal, and Y. Silberberg, "Scanningless depth resolved microscopy," *Opt. Express* **13**, 1468-1476 (2005).
13. E. Tal, D. Oron, and Y. Silberberg, "Improved depth resolution in video-rate line-scanning multiphoton microscopy using temporal focusing," *Opt. Lett.* **30**, 1686-1688 (2005).
14. G. Zhu, J. van Howe, M. Durst, W. Zipfel, and C. Xu, "Simultaneous spatial and temporal focusing of femtosecond pulses," *Opt. Express* **13**, 2153-2159 (2005).
15. E. Papagiakoumou, V. de Sars, D. Oron, and V. Emiliani, "Patterned two-photon illumination by spatiotemporal shaping of ultrashort pulses," *Opt. Express* **16**, 22039-22047 (2008).
16. J. W. Goodman, *Introduction to Fourier Optics, third edition* (Roberts and Company, Greenwood Village, 2005).
17. D. Oron and Y. Silberberg, "Harmonic generation with temporally focused ultrashort pulses," *J. Opt. Soc. Am. B* **22**, 2660-2663 (2005).
18. G. J. Brakenhoff, J. Squier, T. Norris, A. C. Bliton, M. H. Wade, and B. Athey, "Real-time two-photon confocal microscopy using a femtosecond, amplified, Ti:Sapphire system," *J. Microsc.* **181**, 253-259 (1995).
19. C. Ventalon and J. Mertz, "Quasi-confocal fluorescence sectioning with dynamic speckle illumination," *Opt. Lett.* **30**, 3350-3352 (2005).
20. E. Tal and Y. Silberberg, "Transformation from an ultrashort pulse to a spatiotemporal speckle by a thin scattering surface," *Opt. Lett.* **31**, 3529-3531 (2006).
21. D. Oron and Y. Silberberg, "Spatiotemporal coherent control using shaped, temporally focused pulses," *Opt. Express* **13**, 9903-9908 (2005).
22. H. Suchowski, D. Oron, and Y. Silberberg, "Generation of a dark nonlinear focus by spatiotemporal coherent control," *Opt. Commun.* **264**, 482-487 (2006).

## 1. Introduction

Generation of complex three-dimensional optical excitation patterns is a requirement in many practical applications, including optical imaging, photoactivation and lithography. Using currently available ultrafast light sources it is simple to localize optical excitation to a point via multiphoton excitation. By scanning this point of excitation (or the excited sample) it is possible to generate arbitrary three-dimensional excitation patterns. Indeed, this is the mode of operation of most multiphoton microscopes [1] and femtosecond lithography systems [2] to date. Such sequential point-by-point scanning of the excitation is, nevertheless, a slow process, despite many attempts to improve scanning systems, for example by the use of acousto-optic deflectors [3, 4]. For some applications such as uncaging of biologically active molecules, the combination of a finite residence and scanning time may be too slow relative to the time scale of the probed process [5]. This, combined with the fact that current-day laser sources typically provide orders of magnitude more power than needed for single-point excitation, is the main driving force behind the development of multiple-point excitation systems [6-11]. Generally, this involves splitting the original beam into several beamlets, each directed to a different point in space. Using beamsplitter arrays, for example [8, 9] this usually results in simple 1D or 2D arrays of illumination points.

Recently, the technique of temporal focusing was introduced as an alternative to axially confine a large multiphoton excitation area to a single plane [12]. Temporal focusing relies on the utilization of geometrical dispersion to produce a short pulse at the image plane of the objective lens, while the pulse is temporally stretched before and after the focus. Therefore, multiphoton processes whose yield is maximized when the peak intensity is highest occur predominantly in the focal plane. Since this principle does not require splitting of the excitation beam into a discrete set of beamlets, temporal focusing enables spatial multiplexing of the excitation while maintaining a continuous excitation profile within the plane. The standard setup, shown in Fig. 1, includes a blazed reflection grating imaged by a high magnification telescope, comprised

of a regular lens and an objective lens, onto the image plane. The grating is illuminated at an oblique angle such that the center frequency of the excitation pulse is diffracted towards the optical axis of the system. It was shown that for a 2D illuminated area ( $\approx 100 \times 100 \mu\text{m}^2$  using a high numerical aperture objective) the axial resolution (corresponding to the extent where multiphoton processes are effectively excited) afforded by temporal focusing is equivalent to that achieved by conventional line-scanning multiphoton excitation. For a two-photon absorption process, this corresponds to the axial response decaying as  $z^{-1}$  away from the focal plane. For a 1D illuminated line (perpendicular to the grating lines), essentially combining temporal focusing with spatial focusing along one spatial dimension, depth resolution is equivalent to that of point scanning [13, 14], recovering the  $z^{-2}$  decay for a two-photon absorption process. These two cases have a closed-form analytic solution.

Both approaches have advantages and inconveniences. The use of a 2D large illumination area allows for a quick acquisition time (provided sufficient excitation intensity), while illumination with a 1D line allows for an increased axial resolution and excitation density. For some applications, excitation configurations that offer a compromise between these two extreme conditions are desirable. One possibility is to use a multiple-line scanning configuration. Alternatively the excitation volume can be limited to a specific region of interest, concentrating the available excitation energy only to this region.

Since temporal focusing relies on imaging of the grating onto the sample, it is reasonable that spatial patterning of the excitation beam on the grating should result in similarly patterned excitation on the sample. 2D patterning of light can be achieved by two means: amplitude only modulation, corresponding to an amplitude mask inserted at the grating surface, or phase-and-amplitude modulation, which practically corresponds to the situation achieved when projecting a digital hologram onto the grating. We have recently implemented the latter scheme, generating a digital hologram by the use of a liquid crystal spatial light modulator (SLM) [15]. The application of a phase pattern on the SLM results in both phase and amplitude modulation of the image on the grating surface. A broadening of the axial response, as well as significant speckle in the temporally focused image were observed in this case.

In this paper we present a generalized numerical and experimental analysis of the effects that light patterning in multiple lines or arbitrary 2D pattern have on the lateral and the axial light distribution. We first briefly present the formalism used for the calculations, and then proceed to analyze the effects on temporal focusing of both 1D and 2D spatial modulation of the excitation beam. In particular we analyze which is, in multiple line excitation, the minimum-line separation that allows maintaining the depth resolution of point scanning. For illumination of a 2D region of interest, we compare the two different modes of illumination corresponding to amplitude only modulation and phase-and-amplitude modulation.

## 2. Calculation of excitation profiles for temporally focused arbitrary excitation patterns

Existing calculations on various effects in temporally focused illumination have generally assumed spatially homogeneous, or at least smooth, illumination patterns. In order to calculate excitation patterns with arbitrary phase- and amplitude- modulated excitation we assume a given complex excitation pattern  $A(x,y)$  which is frequency independent impinging upon the grating at an angle such that the central frequency of the pulse is diffracted perpendicular to the grating surface for oblique plane-wave illumination. The excitation pulse spectrum is then discretized, and the propagation from the grating to the image plane is solved separately for each spectral component using the angular spectrum of waves approach [16], taking into account the finite aperture of the objective lens. This yields a four-dimensional distribution of complex field amplitudes  $A_{\text{image}}(x,y,z,\omega)$ . For each point this is Fourier transformed back into time domain to obtain  $A_{\text{image}}(x,y,z,t)$ , which is then integrated to yield the two-photon excited fluorescence

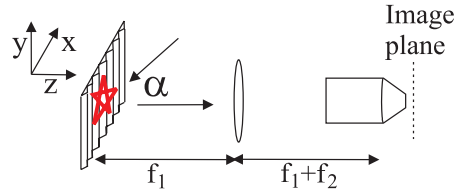


Fig. 1. Setup used for temporal focusing. The grating is aligned perpendicular to the optic axis of a high magnification telescope comprised of a lens and a microscope objective. The excitation beam impinges on the grating at an angle  $\alpha$  such that the center wavelength is diffracted towards the optical axis. An arbitrary pattern is projected on the grating, either via amplitude or phase-and-amplitude shaping. For the latter, the excitation beam is shaped by a spatial light modulator followed by a Fourier lens.

(2PEF) intensity according to Eq. (1), assuming a homogeneous distribution of fluorophores in the entire volume. All calculations were scalar, practically assuming a linear polarization of the excitation beam.

$$I_{2PEF}(x, y, z) = \int_{-\infty}^{\infty} dt |A_{image}(x, y, z, t)|^4 \quad (1)$$

From this, the axial response  $I_{tot}(z) = \int dx dy I_{2PEF}(x, y, z)$ , corresponding to the integrated fluorescence signal from a thin planar fluorescent layer perpendicular to the propagation axis can be easily calculated. The calculations were performed assuming the following parameters (corresponding to experimental conditions detailed elsewhere [15] and also used here, as described in the following): For the 2D case the calculation was performed for a  $100\mu m \times 100\mu m$  area in the XY plane, where the size of each pixel was approximately  $0.25\mu m$ . Along the propagation direction each pixel was  $0.5\mu m$ . The calculation was conducted for a 830 lines/mm grating illuminated at 40.5 degrees from the normal. The focal length of the telescope lens was 50cm, the input aperture of the objective lens was 6mm, and the numerical aperture was 0.9 (corresponding to a sine of the cone angle of 0.6 in the glass or PMMA layer). The pulse spectrum, with a FWHM of 8.5nm, centered at 780nm, was discretized in the calculation to 61 colors spaced in wavelength by about 0.25nm. Both 1D and 2D calculations yielded practically identical results for 1D illumination patterns.

These conditions were chosen in order to directly compare with experimental results for both 1D (see below) and 2D [15] shaped excitation patterns. The presented results are, nevertheless, quite general in their applicability to other focusing condition, using the scaling of temporal focusing Rayleigh range with the excitation numerical aperture:  $b \propto NA^{-2}$  [14, 17]. When considering the sectioning capabilities of temporal focusing, we compare below to two cases: a standard point scanning multiphoton microscope, and a line-scanning two-photon microscope [18].

### 3. Temporal focusing with 1D patterned excitation

As discussed above, simple analytical solutions exist for temporal focusing of either a homogeneously illuminated area or for the case of a thin line perpendicular to the grating lines. It was shown that, at least for incoherent processes such as 2PEF, in the former case the spatially uniform depth resolution is equivalent to that of line-scanning [12], whereas for the latter it is equivalent to that of point scanning [13, 14]. This can be readily understood considering the time-domain picture of temporal focusing. The ultrashort pulse impinging on the grating generates, transiently, an illumination pattern which is its geometrical crossing with the grating. The

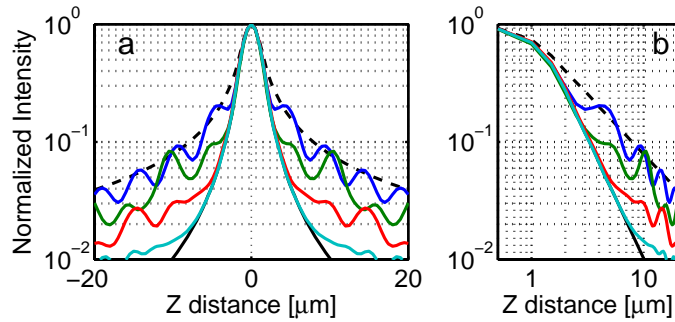


Fig. 2. Depth response for illumination gratings with varying ratios of  $\Delta y/2Mw_0$ : 5 (blue); 7.5 (green); 12.5 (red); 20 (cyan). Also plotted is the calculated response for an area (dashed black line) and for a single line (solid black line).

cross of two planes (the grating and a pancake-shaped ultrashort pulse) yields a line, whereas that of a plane (the grating) and a line (in the case of line illumination) yields a point. In the following we consider how the transition between these two regimes occurs. In particular, one can ask what is the achievable depth resolution with patterned illumination perpendicular to the grating lines.

To address this we consider the case of illumination by an array of equally spaced lines such that each of these lines is demagnified by the telescope to a diffraction-limited line (corresponding to  $2w_0 \approx 0.4\mu m$  in our case).

Let us start by considering the simplest case of an array of lines of equal intensity and constant phase. Clearly in this case choosing a large spacing  $\Delta y$  between lines should reproduce the single line illumination limit, while choosing  $\Delta y$  to be of the order of  $2Mw_0$ , where  $M$  is the telescope magnification, should reproduce the area result. In Fig. 2(a) we plot the integrated 2PEF signal  $I_{tot}(z)$  as a function of the propagation length for various ratios of  $\Delta y/2Mw_0$ . A similar curve on a log-log scale, outlining the inverse power-law dependence of the axial response at large  $z$ , is given in Fig. 2(b) (for positive values of  $z$ ).

As can be seen, the depth response near  $z=0$  (and the axial FWHM) rapidly converges from that of line scanning (dashed black line) to that of point scanning (solid black line) even for a ratio of 5. The response at larger  $z$ , however, decays more slowly and shows an oscillatory pattern. Closer inspection yields that the peaks are equally spaced in  $z$ , and their location corresponds to the expected position of Talbot images and subimages at  $z = \frac{nL^2}{2\lambda}$ , where  $n$  is an integer and  $L = \Delta y/M$  [16]. As can be seen, the depth resolution curve follows that of point scanning for  $|z| < \frac{L^2}{2\lambda}$  (the spatial position of the first Talbot subimage) and decays more slowly thereafter. As long as the first Talbot subimage is more than approximately two Rayleigh ranges away from the focal plane, corresponding here to a ratio of about 10, the response becomes practically very close to that of point scanning.

A practical way to obtain an illumination pattern of the form described in Eq. 1 is to shape the excitation beam using a spatial light modulator and position the grating at the Fourier plane of a cylindrical lens. A phase grating pattern imprinted on the SLM can then be efficiently converted to an array of lines on the grating. In particular, we consider here a phase pattern of the form  $\Phi(y) = 1.3\cos(ky) + 1.65\cos(2ky)$ , which results in a rather uniform array of seven lines on the grating. In this case, however, the phases vary from line to line. To quantify this we compare both the depth resolution and the resulting YZ illumination pattern for this case with two others: a uniform phase, and a completely random phase. These results appear in Fig. 3 for  $L = 3\mu m$  (a ratio of 7.5).

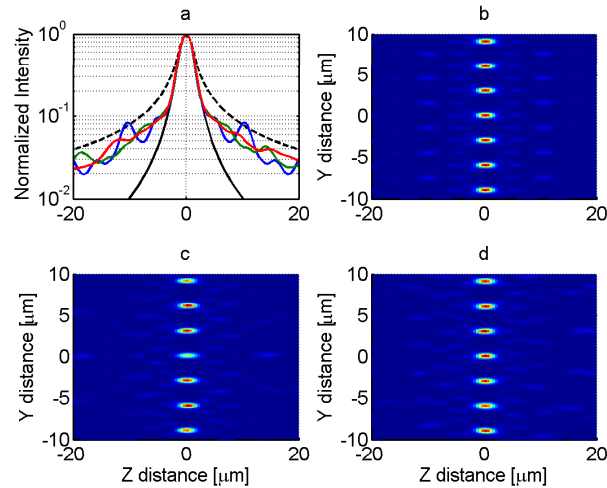


Fig. 3. The effect of phase of lines in an array on the depth response for the case of  $\Delta y/2Mw_0 = 7.5$ . a) Depth response for constant phase (blue), a holographically generated array (green) and a random phase (red), along with the calculated response for an area (dashed black line) and for a single line (solid black line). b)-d) YZ intensity plots for constant phase (b), a holographically generated array (c) and random phases (d).

The  $z$  response curves show a similar trend, but the details appearing in the constant phase calculation, in particular the periodic modulation at Talbot image planes are lost. This is accentuated in the spatial response curves presented in Figs. 3(b)-3(d), where the periodic order of Fig. 3(b) is lost outside the focal plane in Figs. 3(c)-3(d). Still, even for the random phase case it can be seen that the  $z$  response follows that of point illumination up to the expected location of the first Talbot subimage and slowly decays thereafter.

We performed an experimental test of the expected  $Z$ -response of a holographically generated array of temporally focused lines similar to that described in Fig. 3(c). The experimental setup has been detailed elsewhere [15]. Briefly, pulses from a Ti:Sapphire laser oscillator are directed towards a phase-only spatial light modulator (SLM). A Fourier lens projects the generated digital hologram onto a grating. The grating is then imaged onto the sample using a telescope comprised of an achromatic lens and a microscope objective. A thin layer of Rhodamine dye in PMMA is scanned in the vertical dimension, and imaged with a second objective onto a cooled CCD camera. In the current experiment, the phase pattern on the SLM was modulated only in the vertical dimension, and the Fourier lens used was a cylindrical one. This resulted in an illumination pattern in the form of an array of lines on the grating. The corresponding experimental  $z$  response for several values of  $\Delta y/2Mw_0$  to be compared with the predictions of Fig. 2 is presented in Fig. 4. As can be seen, in agreement with the above predictions, the depth response for all values of  $\Delta y/2Mw_0$  generally follows the single line depth response (black line) around  $z=0$ , with significant deviations appearing only after moving beyond the axial position of the first Talbot subimage.

#### 4. Temporal focusing with 2D patterned excitation

The above discussion dealt with simple illumination patterns which did not interfere with the efficiency of the temporal focusing process. This is due to the fact that the excitation pattern (or more importantly, its phase) was invariant (or, in practice, slowly varying) along the direction perpendicular to the grating lines. In practice, this means that the wavefront of the pulse was

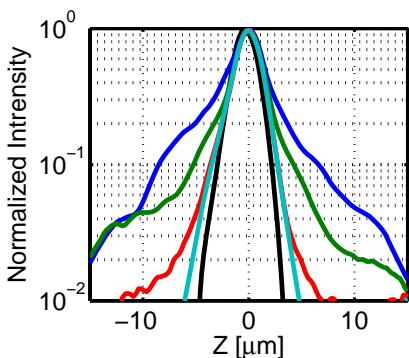


Fig. 4. Experimental realization of illumination by equally spaced lines. The depth response is presented for illumination with a holographically generated array of seven lines with varying ratios of  $\Delta y/2Mw_0$ : 5 (blue) ; 7.5 (green) ; 12.5 (red) ; 20 (cyan). Also plotted is the measured response for a single line (solid black line).

not distorted and the simple time-domain picture described above (of a pancake-like ultrashort excitation pulse) was still valid. This is not necessarily the case for general 2D illumination patterns. In the following we present calculations on the effects of 2D patterning on temporally focused illumination.

Two-dimensional patterns can generally be constructed by two means. Amplitude modulation of the excitation beam impinging on the grating yields intensity variations while maintaining the pulse front flat. On the other hand, the use of phase elements distorts the pulse front. This is typically performed with a computer controlled SLM, having both the grating and the SLM at the two foci of a lens such that the illumination pattern on the grating is the Fourier transform of the applied phase pattern. In this case, generation of an arbitrary two-dimensional pattern on the grating plane (the Fourier plane of the SLM) requires the use of an optimization procedure, such as the Gerchberg-Saxton algorithm. Sharp details in the intensity pattern are typically associated with strong phase modulation across the image, corresponding to a highly distorted pulse front. In the following we discuss the consequences of both regimes of patterning on the axial localization of excitation by temporal focusing.

Let us first discuss temporal focusing for the simpler case of a pure intensity modulation. Since the pulse front is flat, this is generally analogous to the 1D discussion of the previous section, applied sequentially to differently shaped lines within the excitation pattern. Perhaps the simplest such modulation is achieved when the imprinted image on the grating contains sharp edges. Shown in Fig. 5(a) is the intensity pattern at the image plane upon illumination of the grating with a homogeneous circle with sharp edges. Clearly, for every line in the  $y$  direction we observe the diffraction pattern of the sharp edge, which interferes with the circle pattern. Looking at the corresponding FWHM of the axial response at each point, shown in Fig. 5(b), we clearly see that the FWHM is minimal at the intensity peaks and maximal at the intensity minima. Considering the results of the previous section, where depth resolution was improved by excitation with an inhomogeneous pattern (an array of lines) relative to the case of homogeneous illumination (excitation of an entire area), this is a rather intuitive result.

A similar trend is observed for a circle with a random intensity modulation (where the intensity at the grating surface was randomly chosen between 0.5 and 1 for every region corresponding to a demagnified pixel of  $0.25 \times 0.25 \mu\text{m}^2$ , such that it corresponds to a little less than a diffraction limited spot at the image plane). While this case, plotted in Fig. 5(c)-5(d), is not relevant to any practical realization of temporal focusing, it is highly instructive in showing

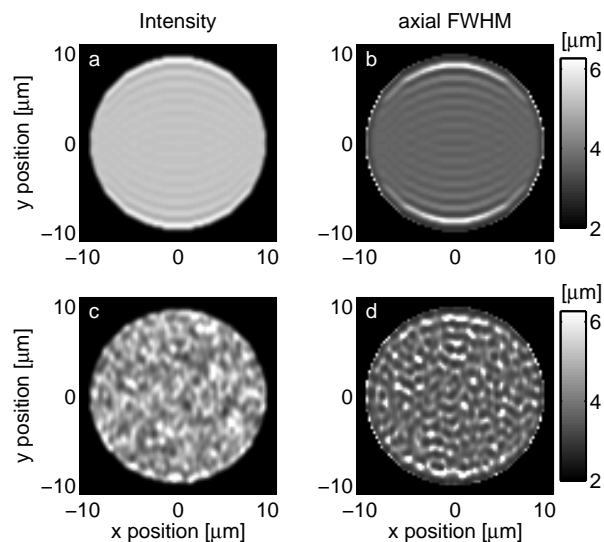


Fig. 5. 2PEF intensity patterns (a,c) and calculated local FWHM (b,d) for two cases having constant spatial phase: A circle with sharp edges (a,b) and a circle with random intensity fluctuations (c,d).

the spatial correlation between intensity peaks and a narrower axial response. It is important to note, however, that for the random pattern presented here the modulation pitch is small (that is, the distance between peaks is such that the effective Talbot peaks are within the rayleigh range of the temporally focused beam). Thus, the integrated  $z$  response shows no improvement relative to that of a homogeneously illuminated area. These results, exhibiting a narrower FWHM at the intensity peaks of the excitation pattern, are closely related to the improved depth resolution achieved in linear microscopy by dynamic speckle interference [19], where a depth-resolved image is digitally formed by taking the variance of the collected emission for several consecutive frames, which is largest at the focal plane.

The situation is more complex when considering phase modulated excitation. As long as the phase varies smoothly (that is, there is little phase variation over a distance of the demagnified diffraction limited spot) the temporal focusing process is hardly affected. Rapid phase variations lead, however, to broadening of the distribution of scattering angles for each color, as observed in our recent experimental study [15]. This both interferes with the geometrical dispersion which lies at the basis of the temporal focusing process and results in significant scattering of light outside the back aperture of the objective lens, generating a speckle pattern at the image plane. The limit of pure phase modulation has previously been discussed both theoretically [12] and experimentally [20] for the case of head-on excitation through a diffuser (which replaces the grating). It was shown that this results in generation of spatiotemporal speckle at the image plane, stretching, along the propagation direction, to a distance of the order of the spatial extent of the undistorted pulse  $c\tau_{pulse}$ . The case of a grating illuminated with a rapidly varying phase pattern is more complex. The intensity pattern at the image plane obtained from a calculation for random phases (where the intensity at the grating surface was maintained constant but the phase was randomly chosen between 0 and  $2\pi$  for every region corresponding to a demagnified pixel of  $0.25 \times 0.25 \mu m^2$ ) is shown in Fig. 6(a). As can be seen, a speckle pattern with rather isolated peaks is generated. The corresponding  $z$  response curve is shown in Fig. 6(b) (solid blue line). It shows a  $4.5 \mu m$  FWHM axial response which is broader than the  $3.3 \mu m$  one obtained for a

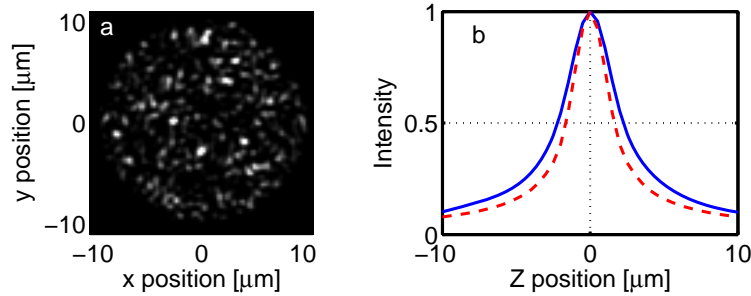


Fig. 6. 2PEF intensity pattern (a) and calculated depth response (b) for an illumination pattern with random phase. The observed FWHM depth response of  $4.5\mu\text{m}$  (solid blue line) is broader than the  $3.3\mu\text{m}$  FWHM response observed for the case of a constant phase (dashed red line).

pure intensity modulation (dashed red line). These values should be compared with the limiting values of the axial response in a line-scanning and point-scanning two-photon microscope using the same numerical aperture of excitation, corresponding to  $2.8\mu\text{m}$  and  $1.7\mu\text{m}$ , respectively.

We now consider in more detail the origin of this broadening. Clearly, the observed intensity peaks, corresponding to most of the generated signal, arise from regions on the grating where more light is diffracted into the objective back aperture. This necessarily means that the phase pattern on the grating in these regions is rather smooth. It is thus expected that locally within these regions the depth resolution should be high. Indeed, when performing a statistical analysis of the distribution of depth resolution vs. maximal signal intensity this trend is observed, as shown in Fig. 7(a). The FWHM observed for the highest intensity points is significantly narrower than the overall averaged response. As can be seen in Fig. 7(b), where we plot the center position between the two points defining the FWHM. Unlike the case of amplitude modulation, where the center position remains at  $z=0$  independent of the signal intensity, here the interference with the background spatiotemporal speckle can shift it within a range of  $\pm 1\mu\text{m}$ . Overall, then, the broad depth response has two origins: one is the nonlinear signal due to the temporal speckle at the wings. The other is the offset of the speckle peak from the  $z = 0$  plane due to interference with the background temporal speckle. Thus, despite the narrow response at each peak, the average response is broadened.

The above results are rather general even in the case of less random phase distributions. In particular, we have tested both numerically and experimentally excitation patterns generated by a Gerchberg-Saxton algorithm converting a Gaussian intensity distribution to several arbitrary intensity patterns. The observed intensity distributions at  $z=0$  as well as the depth response have been reported elsewhere [15]. There, the FWHM of the axial response of the digital hologram was about  $5\mu\text{m}$  as compared with a  $3.2\mu\text{m}$  response obtained with flat-phased modulation, in very good agreement with the predictions of Fig. 6(b). In fact, without imposing any limitations on the phase on the grating plane, the results from an excitation pattern generated by a Gerchberg-Saxton algorithm are almost similar to the case of a pure random phase. Thus, in terms of the axial response, this presents a new limiting case which is an intermediate between the two geometries presented in Ref. 11, that of a pulse impinging head-on onto a diffuser, and that of a flat-phased pulse impinging on a grating at the appropriate angle.

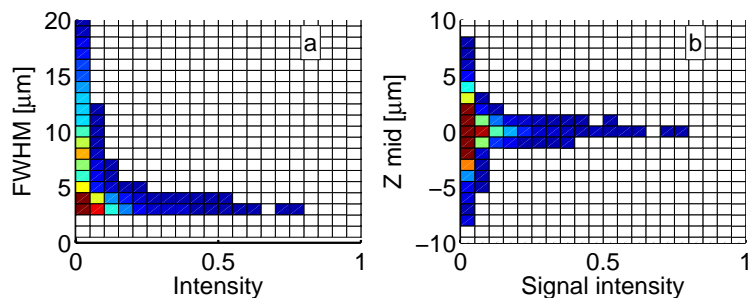


Fig. 7. The origins of broadening of the depth response in temporal focusing with random phase. a) Two-dimensional probability histogram of the depth response FWHM and the signal intensity. Strong intensity is correlated with a narrow response. b) Two-dimensional probability histogram of the centroid of the depth response and the signal intensity. The peak of the signal is not necessarily centered at  $z=0$  even for high signal intensities.

## 5. Conclusion

We have considered the effects of 1D and 2D spatial modulation of temporally focused excitation patterns on the excitation pattern itself and on the axial resolution. The 1D analysis sets a limit on the amount of scanning necessary in order to fully cover a 2D area while maintaining the depth resolution of point scanning. Practical full-field imaging can be achieved by using approximately 10 different illumination patterns (of shifted gratings having a separation of 10 diffraction-limited units in between them). This is an upper limit on the amount of required scanning since we have not considered, for example, polarization effects which can aid in reducing the crosstalk between neighboring excitation lines, or alternatively the use of temporal multiplexing, as is done both for beamsplitter arrays and for microlenses.

Moreover, we show that of the two general schemes which can be utilized to generate 2D illumination patterns, pure amplitude modulation leads to better axial confinement of the excitation and to reduced intensity variations in the projected excitation pattern. In this case, the axial confinement is practically similar to that of a two-photon line scanning microscope. For pure amplitude modulation the axial response may vary across the illumination pattern, with thin isolated lines perpendicular to the grating grooves exhibiting improved axial confinement. Amplitude modulation is, however, clearly inefficient as it leads to loss of excitation power. In addition, care has to be taken to eliminate artifacts induced by sharp edges.

The axial localization of the excitation does not, however, significantly deteriorate even for the limiting case of a random phase, which is a reasonable approximation to the situation of a complex illumination pattern generated by an optimization algorithm such as Gerchberg-Saxton without imposing additional requirements on the phase. We find that in this case the axial resolution is worse by several tens of percent than that of a line scanning multiphoton microscope. Phase modulation can lead to the generation of a speckle pattern in the image plane, also resulting in a loss of excitation intensity (as part of the excitation light does not enter the back aperture of the objective lens).

We thus present here a guideline which can be utilized when generating complex illumination patterns using SLMs. In particular, the depth response as well as the amount of speckle in the image plane depends on the existence of rapid phase variations in the excitation pattern. The absence of these can be demanded as an extra requirement from the search procedure for the phase pattern on the SLM, compromising the exact intensity pattern for improved axial resolution and reduced speckle.

This manuscript has only dealt with a scalar model, not considering the possibilities of varying the spatial polarization or, more interestingly, the combination of spatial shaping with the axial control afforded by temporal shaping [21, 22] to generate complex 3D excitation patterns, although these clearly present new possible applications of temporal focusing. Overall, we believe that the combination of temporal focusing with complex illumination patterns can find application, in particular, in multiphoton lithography and in uncaging experiments.

### **Acknowledgments**

This work was supported by the ESF and the CNRS through the EURYI program, by the European Commission FP6 Specific Targeted Project "PHOTOLYSIS" LSHM-CT-2007-037765 and by the Israeli Science Foundation (Grant No. 1621/07).